Multi-scale tracking reveals scale-dependent chromatin dynamics after DNA damage

Judith Miné-Hattab[a,b,c,†,*], Vincent Recamier[a,†], Ignacio Izeddin[a,d], Rodney Rothstein[b,*], and Xavier Darzacq[a,e,*]

[a]Institut de Biologie de l'Ecole Normale Supérieure (IBENS), 75005 Paris, France; [b]Department of Genetics & Development, Columbia University Medical Center, New York, NY 10032; [c]Nuclear Dynamics, CNRS UMR 3664, Institut Curie, 75005 Paris, France; [d]Institut Langevin, CNRS, ESPCI Paris, PSL Research University, 75005 Paris, France; [e]Division of Genetics, Genomics & Development, Department of Molecular and Cell Biology, University of California, Berkeley, Berkeley, CA 94720

ABSTRACT **The dynamic organization of genes inside the nucleus is an important determinant for their function. Using fast DNA tracking microscopy in *Saccharomyces cerevisiae* cells and improved analysis of mean-squared displacements, we quantified DNA motion at time scales ranging from 10 ms to minutes and found that following DNA damage, DNA exhibits distinct subdiffusive regimes. In response to double-strand breaks, chromatin is more mobile at large time scales, but, surprisingly, its mobility is reduced at short time scales. This effect is even more pronounced at the site of damage. Such a pattern of dynamics is consistent with a global increase in chromatin persistence length in response to DNA damage. Scale-dependent nuclear exploration is regulated by the Rad51 repair protein, both at the break and throughout of the genome. We propose a model in which stiffening of the damaged ends by the repair complex, combined with global increased stiffness, act like a "needle in a ball of yarn," enhancing the ability of the break to traverse the chromatin meshwork.**

Monitoring Editor
Kerry S. Bloom
University of North Carolina

Received: May 23, 2017
Revised: Jul 21, 2017
Accepted: Aug 2, 2017

INTRODUCTION

The dynamic organization of the nuclear genome is essential for many biological processes and is often altered in cells from diseased tissue (Misteli, 2010). Recent advances in live cell imaging make it possible to visualize the dynamic organization of chromosomal loci inside living nuclei (Bronshtein Berger *et al.*, 2013). In the presence of double-strand breaks (DSB) in *Saccharomyces cerevisiae* and some mammalian cell lines, DNA mobility is greatly increased (Dimitrova *et al.*, 2008; Chiolo *et al.*, 2011; Jakob *et al.*, 2011; Dion *et al.*, 2012; Miné-Hattab and Rothstein, 2012; Neumann *et al.*, 2012; Roukos *et al.*, 2013; Lawrimore *et al.*, 2017). In diploid yeast, increased mobility following DSBs likely favors pairing between homologues during repair by homologous recombination (HR) (Miné-Hattab and Rothstein, 2012). In addition, in response to random DSBs in diploid yeast, undamaged loci also exhibit increased mobility albeit to a smaller extent than the damaged locus. Increased mobility of undamaged loci is called global or genomewide increased mobility (Miné-Hattab and Rothstein, 2012, 2013). In haploid yeast, increased mobility following DSBs is also observed even in the presence of nonrepairable DSBs: such an increased mobility is thought to promote ectopic repair events (Neumann *et al.*, 2012). In mouse cells, DSBs exhibiting increased mobility are the source of chromosomal translocations (Roukos *et al.*, 2013). Thus increased DNA mobility in response to DNA damage acts as a double-edged sword since it promotes homologous pairing but in some cases also it leads to potentially mutagenic DNA repair events.

This article was published online ahead of print in MBoC in Press (http://www.molbiolcell.org/cgi/doi/10.1091/mbc.E17-05-0317) on August 9, 2017.

†These authors contributed equally.

Author contributions: J.M.-H. designed and performed the experiments, analyzed and interpreted the data, made the figures, wrote the manuscript, and coordinated the project. V.R. developed the improved fitting analysis of MSD curves, helped in the interpretation of the data, and helped in the preparation of some figures. I.I. worked on the conception of the microscope, helped in the interpretation the data, and helped in writing the manuscript. R.R. cowrote the manuscript. X.D. helped in the interpretation of the data.

*Address correspondence to: Xavier Darzacq (darzacq@berkeley.edu), Judith Miné-Hattab (judith.mine@curie.fr), or Rodney Rothstein (rothstein@columbia.edu).

Abbreviations used: DSB, double-strand break; HR, homologous recombination; MSD, mean-squared displacement; SC, synthetic culture.

As chromosome mobility is an important facet of the DNA damage response, investigating the nature of DNA diffusion in the context of repair is essential to understand how cells maintain their genome integrity. The mode of diffusion of a moving object drastically changes the way it explores the available space and the time to reach a specific target destination (Guerin *et al.*, 2012). Thus the kinetics of colocalization between two biological entities strongly depends on how these entities diffuse. One method to characterize DNA mobility consists of fluorescently marking chromosomal loci, measuring their displacement over time, and calculating their mean-square displacement (MSD) (Meister *et al.*, 2010). The MSD curve represents the amount of space a locus has explored in the nucleus, and its shape reveals the nature of DNA motion. When a particle freely diffuses, its MSD curve is linear with time and its motion is called "Brownian." However, in living cells, DNA motion is often slower than Brownian diffusion and is called "subdiffusive" (Barkai *et al.*, 2012). Several types of subdiffusive motion have been observed. When a chromosomal locus is confined inside a subvolume of the nucleus, the motion is called *confined subdiffusion* and the MSD exhibits a plateau (Marshall *et al.*, 1997). When the force or structure that restricts the motion is not a simple confinement but is modulated in time and space with scaling properties, the motion is called *anomalous subdiffusion* (Barkai *et al.*, 2012; Metzler *et al.*, 2014). In this case, subdiffusive loci are constrained, but, unlike confined loci, they can diffuse without boundary and thus reach further targets if given enough time. For subdiffusive motion, the MSD exhibits a power law (MSD ~ At^{α}), where α, the anomalous exponent, is smaller than 1. The anomalous exponent α is linked to the degree of recurrence of DNA exploration, that is, the number of times a DNA locus reiteratively scans neighboring regions before reaching a distant position (Ben-Avraham, 2000). When α is small, the locus explores recurrently the same environment for a long time, while a large α indicates that the locus is able to explore new environments often. The anomalous diffusion coefficient A represents the amplitude of DNA motion; it is proportional to the diffusion coefficient only in the case of normal diffusion (when $\alpha = 1$), which is rarely observed in biological systems (Barkai *et al.*, 2012). Previous DNA mobility studies reported confined diffusion (Marshall *et al.*, 1997; Heun *et al.*, 2001; Taddei *et al.*, 2006; Maeshima *et al.*, 2010; Masui *et al.*, 2011; Backlund *et al.*, 2015) while others have reported anomalous diffusion (Maeshima *et al.*, 2010; Weber *et al.*, 2010; Burnecki *et al.*, 2012; Hajjoul *et al.*, 2013; Lucas *et al.*, 2014; Backlund *et al.*, 2015). These studies have been realized with different microscopy techniques and illumination settings. When studying the diffusion of a specific locus, the time scale at which the data are collected translates into the spatial scale of the exploration studied. So far, no consensus has yet been reached to describe the nature of DNA motion probably because different studies interrogate different spatiotemporal scales and therefore interrogate potentially different processes.

Here we have investigated DNA mobility at different time scales ranging from milliseconds to minutes using rapid time-lapse imaging in living *S. cerevisiae* cells. We observe that DNA motion is subdiffusive at time scales ranging from milliseconds to a few minutes, with an anomalous exponent of 0.5 stable at multiple scales in diploid yeast. However, in response to DSBs, DNA mobility is dramatically altered in a different manner depending on the time scales. Damaged DNA loci exhibit distinct anomalous regimes with increased mobility at large time scales but surprisingly reduced mobility at shorter time scales (less than 10 s). Importantly, the presence of distinct regimes of diffusions is not an intrinsic property of the damaged locus: In the presence of random DSBs, undamaged loci also exhibit increased mobility at large time scales and reduced mobility at short time scales. In light of polymer physics, such a pattern of dynamics has been predicted when chromatin persistence length globally increases (Faller and Müller-Plathe, 2008), indicating that chromatin undergoes a general stiffening in response to DSB. Rad51, a central protein of homologous recombination, is required for local and global changes in mobility/stiffening. We propose that global chromatin stiffening following DSBs facilitates nuclear exploration by the damaged DNA ends bound by the Rad51 protein.

RESULTS

DNA mobility exhibits anomalous regimes at different time scales

To characterize DNA dynamics at different time scales, we used diploid cells with a locus fluorescently marked by the insertion of a tet-Operator (*tetO*) array at *URA3* (chromosome V). This *tetO* array is bound by Tet-Repressors, which are fused to red fluorescent proteins (TetR-RFP). We also tagged a structural component of the spindle pole body (SPB) with yellow fluorescent protein, Spc110-YFP, to serve as a marker of the relative nuclear position and to correct for drifting during image acquisition for time intervals longer than 100 ms. Rad52, an essential homologous recombination protein, is fused to cyan fluorescent protein (CFP) to detect the presence of DSB (Figure 1, A and B) (Miné-Hattab and Rothstein, 2012). We selected early S-phase cells with a single SPB (~10% of the total population), and where the *tetO*/TetR-RFP and Spc110-YFP foci are in the same focal plane. We recorded two-dimensional movies of these cells (see Supplemental Movie 1). To avoid cells with spontaneous DNA damage, we ensured that they did not contain a Rad52 focus. Cells were imaged at three time scales:

1. 10-ms time intervals (5-ms exposure time in RFP, no YFP data were acquired since the global movement of the nucleus is negligible during this interval),
2. 100-ms time intervals (50-ms exposure in RFP followed by the same exposure in YFP to track the *URA3* locus and the SPB, respectively),
3. 1000-ms time intervals (500-ms exposure in RFP followed by the same exposure time in YFP).

All acquisitions were performed with doses of light below the threshold of phototoxicity (0.2 J/cm^2; Logg *et al.*, 2009). We measured the *x* and *y* positions of the *lacO*/LacI and the SPC110 spots using a Gaussian fit (see *Materials and Methods*) and we estimated the upper bound of the localization accuracy (including the localization error and the motion blur) at 80 nm (Supplemental Figure S1A, Supplemental Table S1). Supplemental Figure S1A is an example of drift-corrected trajectory of the *tetO*/TetR-FRP that displays no significant change in movement. To assess the nature of its diffusion, we calculated the ensemble-averaged MSD using up to one-third of the shortest trajectory, which represents 70–100 time points. Supplemental Figure S2 shows that it is equivalent to measure the mobility at 100-ms time intervals using continuous illumination (50-ms exposure time in RFP followed by 50 ms in YFP) or discrete illumination (5-ms exposure time in RFP, followed by 5 ms in YFP and 90 ms of lag time). In addition, we mimicked acquisitions at 100-ms time intervals by averaging data acquired at 10 ms over 10 points and obtained similar MSD curves, allowing us to discard any phototoxicity effects.

At the three time scales examined, the MSD curves show bending in linear scale suggesting subdiffusion (Figure 1C). The three MSDs curves are plotted together in log-log scale to allow their simultaneous visualization (Figure 1C, last panel). Since a power-law curve can be mistaken for an exponential form that would account

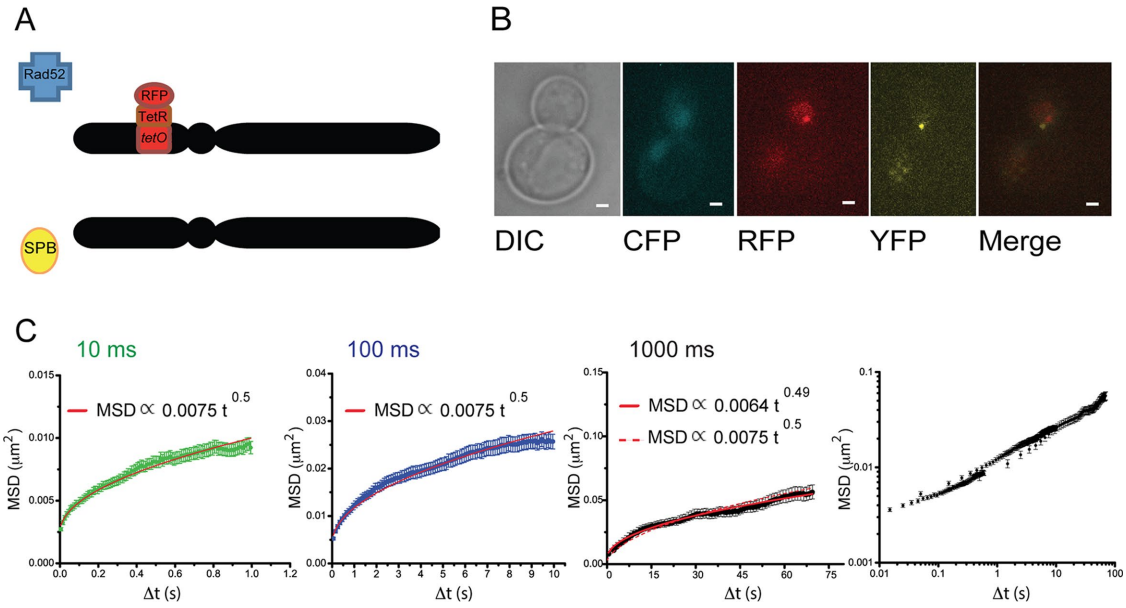

FIGURE 1: Mobility in diploid cells at different time scales. (A) Schematic of the strain: Cells are diploids containing a *tet*O array (3 × 112 copies) inserted at *URA3* (chromosome V). In addition, the Rad52, TetR, and Spc110 proteins are tagged with CFP, RFP, and YFP, respectively. Cells with the *tet*O locus and the SPB in the same focal plane are selected and the *tet*O locus is tracked in two dimensional over time using the SPB as a reference. (B) Typical transmitted, CFP, RFP, YFP and merge images of the cells used for the experiment. The experiment is performed on S-phase cells without a DSB as shown by the absence of a Rad52 focus. The scale bar is 1 μm. (C) Time and ensembled MSD of the *tet*O locus measured at 10-ms time intervals (first panel), 100-ms time intervals (second panel), 1000-ms time intervals (third panel). The fourth panel shows the merge of the three time scales plotted in log-log scale.

for confined diffusion, we used several methods to confirm the anomalous nature of DNA motion (Supplemental Figure S3). We then fitted our MSD curves with a power law. As experimental MSDs are altered by several artifacts (Kepten *et al.*, 2013; Backlund *et al.*, 2015), to fit MSD curves, we use an improved model that takes into account locus mobility during image acquisition and limited position accuracy, the latter (~90 nm) displaying little variation between conditions (see *Materials and Methods*, Supplemental Text 1 and 2 and Supplemental Figure S4). Our approach is similar to the one described in Kepten *et al.* but also includes exposure time as an additional parameter. In addition, we used the "multi-time scale fitting" approach described in Supplemental Text 2. For diploid cells, we obtain MSD(t) ~0.0075 $t^{0.5}$ at 10- and 100-ms time intervals (R_2 = 0.995 and 0.996, Figure 1C). At large time scales (1000-ms time intervals), we observe a different anomalous diffusion coefficient *A* (MSD[t] ~0.0064 $t^{0.49}$, R_2 = 0.992; Figure 1C), likely due to a transition toward confined motion previously observed at larger time scales (10-s time intervals) (Miné-Hattab and Rothstein, 2012).

Since DNA mobility has been investigated in G1 haploid cells using a multi-time-scale approach (Hajjoul *et al.*, 2013), we also measured DNA mobility in haploid cells containing a *tetO*/TetR-RFP array at *URA3* and the Spc110-YFP marked SPB (Supplemental Figure S5, A and B). S-phase haploid cells harboring a single SPB were imaged at the three time scales (10-, 100-, and 1000-ms time intervals). Similarly to our observations in diploid cells, haploids follow subdiffusive motion; however, unlike diploids, a 0.5 anomalous exponent is not seen at all time scales (Supplemental Figure S5, C–E). Indeed, at 10-ms time intervals, we observe a different regime with MSD(t) ~0.011 $t^{0.38}$ (R_2 = 0.999; Supplemental Figure S5C). Our results show a significant cell-to-cell variability (Supplemental Figure S6, A–C) consistent with previous studies (Bronstein *et al.*, 2009; Therizols *et al.*, 2011). Importantly, statistical analysis of the anomalous exponent (Supplemental Figure S6, D–F) shows that the different exponents measured here are not due to insufficiencies in the data set but rather reflect the existence of distinct anomalous regimes of the *URA3* locus depending on the time scale. Strikingly, a significant increase of the global MSD in haploids is seen compared with diploids at every exposure time investigated, as indicated by the higher values of the anomalous diffusion coefficient *A* in haploids (Supplemental Figure S5F).

Table 1 presents a summary of the results obtained in both diploids and haploids. Overall the motion of the *URA3* locus is subdiffusive for time scales ranging from milliseconds to minutes and is well fit by a 0.5 anomalous exponent in most conditions. However, a universal regime is not sufficient to describe DNA motion, since at the very short time scale (10 ms), the anomalous exponent drops to 0.38 in haploids, and at all time scales examined, diploid cells exhibit lower MSD curves than haploids.

At short time scales, damaged DNA is less mobile than in the absence of DSBs

Previous studies have shown that the mobility of a damaged DNA locus increases when its motion is observed at 10-s time intervals in diploids (Miné-Hattab and Rothstein, 2012) and 1.5-s time intervals in haploids (Dion *et al.*, 2012). However, mobility after DNA damage at shorter time scales has never been investigated. Here we measure at multi time scales the mobility of a single I-*Sce*I induced DSB in the same strains used in our previous study (Miné-Hattab and Rothstein, 2012) (Figure 2). We used diploid cells containing the homologous *URA3* loci fluorescently marked with a *lacO*/LacI-YFP and a *tetO*/TetR-RFP array, respectively (Figure 2A). To induce a single DSB, the strain contains an I-*Sce*I target site 4 kb from the

	Time interval (ms)	A	α	R_2
Haploid no damage	10	0.01	0.38	0.999
	100	0.012	0.50	0.997
	1000	0.012	0.50	0.997
Diploid no damage	10	0.0075	0.50	0.995
	100	0.0075	0.50	0.996
	1000	0.0064	0.49	0.992
Diploid with a single DSB (I-*Sce*I induced)	10	0.0064	0.50	0.997
	100	0.0064	0.50	0.995
	1000	0.010	0.58	0.994
Diploid with random DSBs (irradiation with 40 Gy)	10	0.0055	0.5	0.99
	100	0.0055	0.5	0.98
	1000	0.0055	0.5	0.99
	3000	0.0004	1	0.99

The anomalous diffusion coefficients A and the anomalous exponents α were obtained by fitting the D curves with $At^{\alpha} + b$ (see equation 1 from Supplemental Text 1). The parameter b is an experimental offset allowing the correction of artifacts during the acquisition (i.e., localization accuracy and motion blur, see Supplemental Text 1). The fitting method is described in detail in Supplemental Text 2.

TABLE 1: Summary of anomalous motion measurements.

tetO/TetR-RFP locus, as well as RAD52-CFP used as a marker for the presence of the DSB. Cells were incubated in 2% galactose for 90 min to induce the DSB, and induction was stopped by adding 2% glucose. Note that the time of Rad52 focus formation cannot be precisely known; however, all cells were observed after the same incubation time (90 min), when Rad52 foci start to appear (Miné-Hattab and Rothstein, 2012). We next selected S-phase cells harboring a single SPB and a Rad52 focus colocalizing with the *URA3* locus (*tetO*/TetR-RFP) in the SPB focal plane (Figure 2B). We verified that the two homologous *URA3* loci were unpaired by choosing cells with a distant *URA3* homologue (*lacO*/LacI-YFP). The *tetO* and SPB positions were measured over time in two dimensions at three time scales (10, 100, and 1000 ms) using the exact same illumination conditions as in the absence of DNA damage. We then calculated ensemble-averaged MSDs on these cells (Figure 2C).

Similarly to our results in the absence of DSBs, the damaged locus follows anomalous diffusion. At the longest time scale (1000 ms), we find the highest values of A and α in this study (MSD[t] ~0.010 $t^{0.58}$, R_2 = 0.994), indicating increased mobility consistent with previous observations at 10-s time intervals (Miné-Hattab and Rothstein, 2012). Surprisingly, the motion of the damaged locus observed at shorter time intervals exhibits a lower amplitude and anomalous exponent than that seen in undamaged cells, signifying reduced mobility (MSD[t] ~ 0.0064 $t^{0.50}$, R_2 = 0.995 and R_2 = 0.997 at 100- and 10-ms time intervals, respectively, Figure 2C and Table 1). As a consequence, the MSD curve of the damaged locus crosses that of the undamaged one at time t ~ 10 s (Figure 2D). Importantly, all cells are observed during the same stage of DNA repair, that is, when the first Rad52 foci start to appear and homologous loci are unpaired. These cells are examined during 50–150 s depending on the time scale used: This acquisition time is negligible compared with the time necessary for DNA pairing in this system (Miné-Hattab and Rothstein, 2012). Thus the differences in mobility observed here are likely solely due to the different time scales used to observe the damaged locus. A previous study reported reduced motion of chromatin near a DSB during resection (Saad *et al.*, 2014); however, Saad *et al.* compared mobility before damage and during different stages of resection, while we examined mobility during the same stage of repair using different acquisition speeds. Thus both studies investigate different processes.

Overall multi-time-scale imaging of a damaged locus reveals that broken ends are less mobile at short time scales and exhibit different diffusion properties than at other scales. The reduced mobility seen at short time intervals reflects an important property of the damaged end, which might be triggered by the DNA repair machinery itself.

Reduced mobility of the damaged locus at short time scales is Rad51 dependent

Rad51, the central protein of HR, is required for increased mobility of a damaged end at large times scales (Dion *et al.*, 2012; Miné-Hattab and Rothstein, 2012). To test whether *RAD51* is also involved in the reduced mobility that we observe at short time scales, we measured the mobility of a damaged end in *rad51*Δ diploid cells with the exact same illumination settings. Both alleles of the *RAD51* gene in the diploid strain described above were deleted. We then measured the *URA3* mobility in the absence of damage and after 90 min of DSB induction at 10-, 100-, and 1000-ms time intervals. Again, after DSB induction, we selected S phase cells harboring a Rad52 focus colocalizing with the *URA3* locus, a single SPB, and an unpaired distant *URA3* homologue. In the absence of *RAD51*, damaged loci failed to exhibit either increased or decreased mobility, indicating that Rad51 is required for changes in mobility at the damaged site at both short and long time scales (Figure 2E).

Random DSBs also provoke global reduced mobility at short time scales in a Rad51-dependent manner

An important question is whether changes in chromatin conformation and dynamics are localized around the site of damage or also affect the rest of the genome. In diploid yeast, increased mobility in response to DSB is not an intrinsic property of the damaged locus. Indeed, induction of DNA damage on a different chromosome or ionizing irradiation provokes global increased mobility affecting the whole genome (Miné-Hattab and Rothstein, 2012, 2013; Seeber *et al.*, 2013). We thus tested whether reduced mobility over shorter time scales is restricted to the damaged end or can occur genome wide. We used diploid cells with a *tetO*/TetR-RFP at the *URA3* locus, Spc110-YFP, and Rad52-CFP used as a marker for DSBs. We irradiated cells with 40 Gy, equivalent to 4 DSBs per nucleus in average (Ma *et al.*, 2008). We then selected S-phase cells with a single SPB in the same focal plane as the *URA3* locus, as well as a Rad52 focus (Figure 3, A and B). Unlike the previous experiments, Rad52 foci do not colocalize with the *URA3* locus, and since chromosome V represents less than 2% of the genome, the probability of a DSB on that chromosome is extremely low. Immediately following irradiation, we measured the *URA3* mobility at four time scales (10-, 100-, 1000-, and 3000-ms time intervals) and plotted the MSD curves (Figure 3C and Supplemental Figure S7).

At the longest time scale (3000 ms), the MSD of irradiated cells is higher than in the absence of damage, consistent with global increased mobility previously reported at 10-s time intervals (Miné-Hattab and Rothstein, 2012). At 1000-, 100-, and 10-ms time intervals, undamaged loci exhibit a lower amplitude compared with that seen in the absence of DSB, signifying global reduced mobility at these three time scales [MSD[t] ~ 0.0055 $t^{0.5}$, R_2 = 0.99; Figure 3C and Supplemental Figure S6]. As observed at the site of damage,

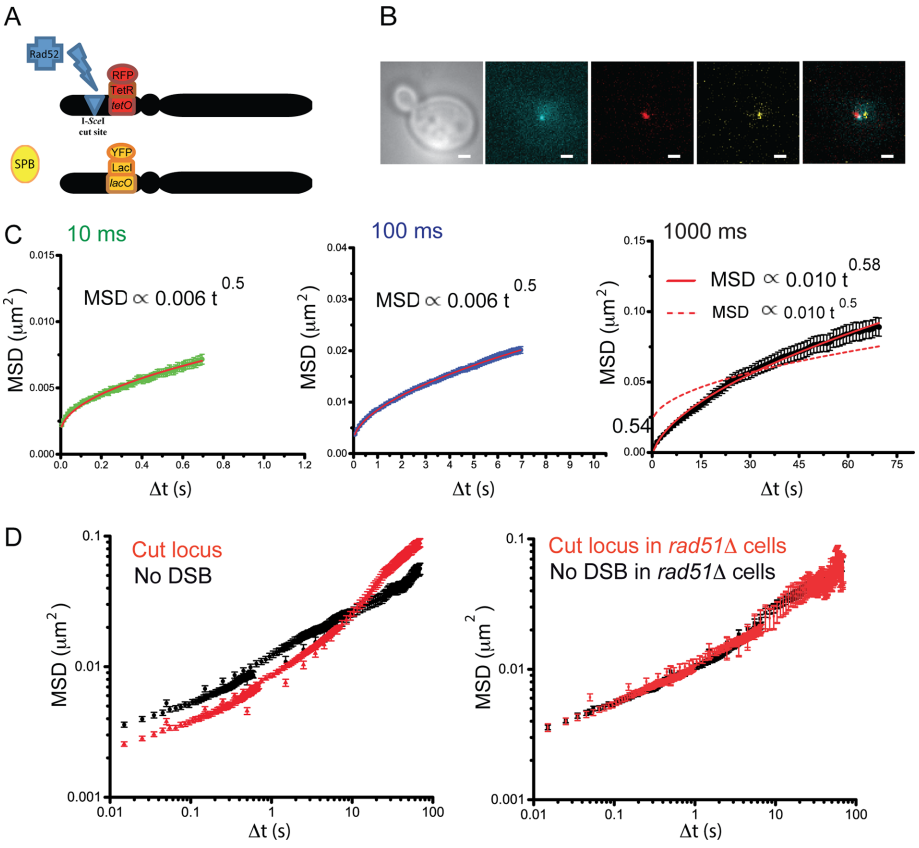

FIGURE 2: Mobility of a single I-*Sce*I induced DSB in diploid cells at different time scales. (A) Schematic of the strain used for the induction of a single DSB in diploid cells. Diploid cells contain both a *tet*O array (3 × 112 copies) at *URA3* (chromosome V) and a *lac*O array (256 copies) at *URA3* on the other homologue. The Rad52, TetR, and LacI proteins are fused with CFP, RFP, and YFP, respectively. A single I-*Sce*I cut-site is located 4 kb from the *tetO* array. A galactose-inducible I-*Sce*I inserted at the *LYS2* locus allows regulated induction of a single DSB under galactose control (Miné-Hattab and Rothstein, 2012). (B) Typical transmitted, CFP, RFP, YFP and merge images of the cells after 90 min of galactose induction. Only S-phase cells containing a Rad52 focus colocalizing with the *tet*O locus and a distant *lac*O focus are selected. The scale bar is 1 μm. (C) Time and ensembled MSD of *tet*O array after induction of a single I-*Sce*I DSB. S-phase cells harboring a Rad52 focus colocalizing with the *tetO*, and a distant homologous locus (*lacO*-LacI-YFP) are selected. The mobility of the *tetO* array is measured at 10-ms time intervals (left panel), 100-ms time intervals (middle panel), and 1000-ms time intervals (right panel). (D) Merge of the three time scales plotted in log-log scale after I-*Sce*I induction (red curves). The MSDs of the *tetO* array in the absence of DNA damage is shown as a reference (black curve, same data as Figure 1C, fourth panel). (E) MSDs of the *tetO* array after induction of a single I-*Sce*I DSB in *rad51*Δ cells. Mobility is measured at 10-ms, 100-ms, and 1000-ms time intervals and the three MSD curves are shown in log-log scale. The mobility of the *tetO* array in the absence of damage in *rad51*Δ cells is also shown (black).

both global increased and global reduced mobility are RAD51 dependent, since irradiated *rad51*Δ cells do not exhibit any increase in mobility (Figure 3D).

DISCUSSION

Multi-time-scale microscopy reveals the composite nature of DNA motion

Previous studies have shown that DNA motion observed at long time scales (1.5- to 10-s time intervals) is confined within a subnuclear volume (Marshall *et al.*, 1997; Heun *et al.*, 2001; Miné-Hattab and Rothstein, 2012). In response to DSBs, DNA becomes more mobile and explores a larger nuclear volume (Dion *et al.*, 2012; Miné-Hattab and Rothstein, 2012). Here, by investigating DNA motion at time scales 10, 100, and 1000 times faster, we find that the MSD curves do not exhibit a plateau indicating that the effect of confinement is not observed at these scales. Instead, the MSD curves are in excellent agreement with a power law, $MSD(t) \sim At^{\alpha}$, a signature of anomalous diffusive motion (Barkai *et al.*, 2012). At the longest time scale studied here (1000-ms time intervals), velocity auto-correlation functions indicate that the motion is not purely anomalous (Supplemental Figure S3D); this time scale likely corresponds to a transition toward confined motion, previously described at 10-s and larger time intervals (Marshall *et al.*, 1997; Miné-Hattab and Rothstein, 2012). In addition, our data show a fundamental difference in DNA mobility between haploids and diploids (Supplemental Figure S5). The anomalous diffusion coefficient *A* is nearly 2 times higher in haploids, indicating that the *URA3* locus is more mobile in haploids. One possible explanation for this difference is that the chromatin in haploid cells is less dense at the *URA3* locus.

In response to a single DSB, we find distinct anomalous regimes depending on the time scales, with both *A* and α increasing between the 100-ms and 1000-ms time intervals experiments (Figure 2 and Table 1). These changes indicate a fundamental difference in the way the damaged locus explores the nuclear space at different time scales. The anomalous exponent α is linked to the degree of recurrence of the motion, low α corresponding to a locus that rescans neighboring loci many times in a highly recurrent manner (Ben-Avraham, 2000; Condamin *et al.*, 2007; Guerin *et al.*, 2016). The anomalous diffusion coefficient *A* reflects the amount of volume explored by a locus as a function of time (i.e., the amplitude of the motion). At 1000-ms time intervals, the higher *A* together with the higher α of the damaged locus indicates that the damaged locus moves with a larger amplitude and in a less redundant manner (Table 1, $A = 0.010$, $\alpha = 0.58$ after I-*Sce*I induction compared with 0.0064 and 0.49 before damage). On the other hand, the low anomalous diffusion coefficient *A* of the damaged locus at 10- and 100-ms time intervals reflects reduced amplitude of the damaged DNA motion (Table 1, $A = 0.0064$ for the damaged DNA compared with 0.0075 in the absence of DSB). These changes in nuclear exploration at the broken end are Rad51 dependent, highlighting the role of Rad51 in regulating chromatin dynamics at the site of damage.

Importantly, the existence of different regimes of diffusion depending on the time scales is not an intrinsic property of the damaged end. In response to random DSBs (40 Gy), we also observe distinct anomalous regimes, with global increased mobility at long time scales and global reduced mobility at short time scales (Figure 3C, Supplemental Figure S6, and Table 1). Interestingly, the MSD curves of cut loci versus loci in undamaged cells cross at 10 s (Figure 2D), whereas the ones in irradiated cells versus undamaged

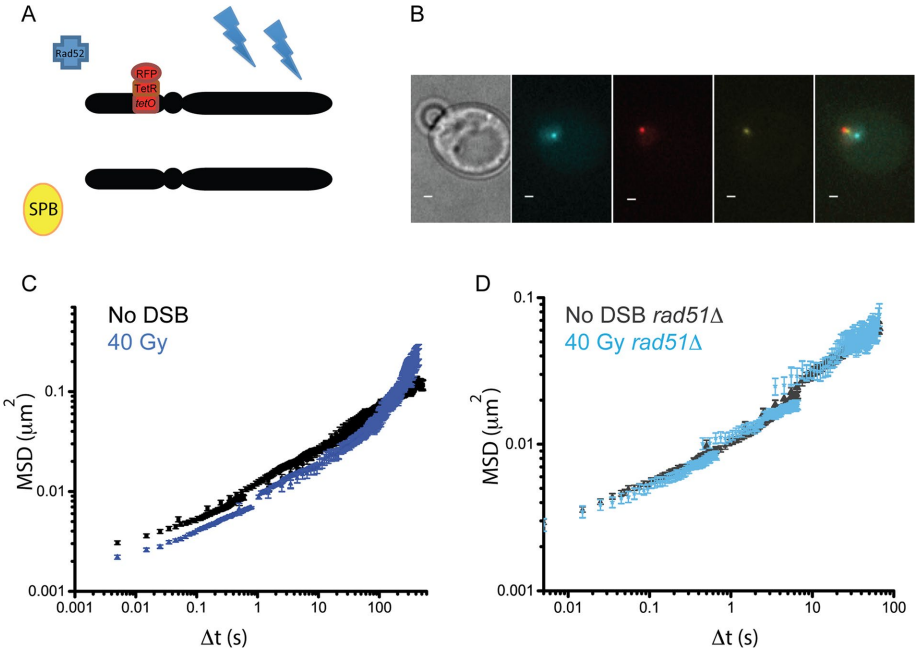

FIGURE 3: Mobility of the *URA3* locus in response to random DSBs (irradiation of 40 Gy). (A) Schematic of the strain: Cells are diploids containing a *tet*O array (3 × 112 copies) inserted at *URA3* (chromosome V). In addition, the Rad52, TetR, and Spc110 proteins are tagged with CFP, RFP, and YFP, respectively. Cells with the *tet*O locus and the SPB in the same focal plane are selected, and the *tet*O locus is tracked in two dimensions over time using the SPB as a reference. (B) Typical transmitted, CFP, RFP, YFP, and merge images of the cells after x-irradiation (40 Gy). Only S-phase cells containing a Rad52 focus are selected. Rad52 foci do not colocalize with the *tetO* array since DSBs are random. The scale bar is 1 μm. (C) MSD curves of the *tetO* array after 40 Gy measured at 10-, 100-, and 1000-ms time intervals (dark blue). The MSDs of the same locus in the absence of DNA damage is shown as a reference (black curve, same data as Figure 1C, fourth panel). (D) MSDs of the *tetO* array after 40 Gy in *rad51*Δ cells. Mobility is measured at 10-ms, 100-ms, and 1000-ms time intervals, and the three MSD curves are shown in log-log scale (light blue). The mobility of the *tetO* array in the absence of damage in *rad51*Δ cells is also shown (black).

cells cross at 100 s (Figure 3C). In other words, it takes 10 s on average for a broken locus to cover larger distances than in the absence of a DSB, allowing the damaged site to reach further targets; in contrast, following random DSBs, the same locus needs 100 s on average to cover larger distances than in the absence of DSBs. Thus, upon DNA damage, changes in mobility have a stronger effect at the damaged locus than in the rest of the genome. This difference suggests that local and global changes in mobility are regulated differently. Overall our findings show that a single mode of diffusion is not sufficient to describe DNA motion at different time scales. Instead, following DSBs, DNA motion is composed of several diffusion regimes that simultaneously drive DNA at each time scale. Such changes in the subdiffusion mode dramatically modify the balance between surrounding and distant chromatin sampling. Thus, in the presence of DNA damage, the existence of multi-time-scale regimes of diffusion may reflect changes in chromatin conformation that increase homology search efficiency.

Origin of subdiffusive motion

Subdiffusive motion has been observed in bacteria, yeast, and human cells, with anomalous exponents ranging from 0.32 to 0.77 (Bronstein *et al.*, 2009; Weber *et al.*, 2010; Hajjoul *et al.*, 2013; Backlund *et al.*, 2014; Lucas *et al.*, 2014). Although different time scales were examined in these studies, none clearly showed the existence of multiple anomalous regimes with the exception of a study by Bronstein *et al.* (2009). In their study, they found that in U2OS cells, diffusion of telomeres is composed of two transient anomalous regimes and becomes close to Brownian at time scales greater than 5 min (Bronstein *et al.*, 2009). Their work emphasizes the importance of the time scale of observation for interpreting DNA motion.

To understand the origin of anomalous subdiffusion of DNA in the nucleus, several models have been proposed as follows:

1) The nucleoplasm is modeled as a visco-elastic medium. Mathematical models of visco-elasticty are fractional Brownian motion and fractional Langevin motion (Metzler and Klafter, 2000). In these models, DNA is subjected to frictional forces that are not proportional to DNA velocity.
2) The nucleoplasm is modeled as a fractal. DNA loci are free explorers moving in a restricted geometry with scale-less properties imposed by nuclear crowding (Condamin *et al.*, 2007).
3) The nucleoplasm is modeled as a polymer melt. DNA loci are represented by monomers whose motion is driven by the properties of this melt. Several polymer models have been suggested to describe DNA mobility, from diluted regimes (Rouse and Zimm models [Andrews, 2014; Vasquez and Bloom, 2014]) to a larger scale semidiluted regime ("tube" model also called "blob" model [De Gennes, 1982]).

Since DNA is a polymer, we compared our experimental anomalous exponents to those obtained in the three polymer models referred to above. The "tube" model of De Gennes is the only one that predicts different regimes of anomalous diffusion arising in a polymer melt (De Gennes, 1982). This model predicts three anomalous diffusion regimes: the Rouse regime at a diluted scale (where $\alpha = 0.5$), the "relaxation of the coil" regime ($\alpha = 0.25$), and by the "reptation" regime ($\alpha = 0.5$) at a semidiluted scale and concentration where adjacent chains constrain the motion. Finally, it predicts Brownian diffusion ($\alpha = 1$) at the macroscopic scale. The reptation regime of this model is obtained by averaging different conformations of polymer entanglements; thus it is the only model that takes into account potential cell-to-cell variability (De Gennes, 1982). This regime has been directly observed in vitro for constrained DNA melts (Perkins *et al.*, 1994); moreover, in live U2OS cell experiments, diffusion of telomeres observed at 1-s time intervals were explained by the reptation regime (Bronstein *et al.*, 2009). Importantly, using the tube model, simulations of polymer dynamics show how global stiffening of polymers affect their dynamics: when the global stiffness of polymers increases, their MSD become lower at short time scales and higher at long time scales (Faller and Müller-Plathe, 2008). As a consequence, the MSD curves before and after global stiffening cross (Faller and Müller-Plathe, 2008).

Our data show that, in most conditions, the anomalous exponent is 0.5. To explain this behavior, we favor the "reptation regime"

versus the Rouse regime for the following four reasons: 1) we observe an anomalous diffusion coefficient *A* in haploids that is double that of diploids; in the reptation regime, this difference in *A* would be well justified by a lower level of chromatin entanglements in haploids compared with diploids, whereas the Rouse regime does not explain it; 2) at the shortest time interval, haploids exhibit a regime with an anomalous exponent lower than 0.5, which may be a transition from *the relaxation of the coil* regime to the reptation regime; 3) we observe high cell-to-cell variability, as predicted by the reptation regime, and more importantly; and 4) modeling the global stiffening of polymers in the reptation regime leads to reduced mobility at short time scales and increased mobility at long scales (Faller and Müller-Plathe, 2008), which is consistent with our experimental observations after DNA damage (Figures 2 and 3).

Linking DNA mobility and chromatin persistence length

The changes in anomalous coefficient *A* that we measure reveal valuable information on chromatin plasticity in response to DSBs. Indeed, in the reptation regimes, where $\alpha = 0.5$, the anomalous diffusion coefficient *A* negatively correlates with the global chromatin persistence length (Faller and Müller-Plathe, 2008). To our knowledge, there is no consensus on the exact equation linking *A* and the persistence length L_p. However, we can qualitatively discuss changes in global persistence length from our MSD measurements. Here we found that on DNA damage, the anomalous diffusion coefficient *A* is smaller at short time scales, resulting in crossing MSD curves between damaged and undamaged cells (Figure 3, Supplemental Figure S7, and Table 1). Such a decrease of *A* is predicted by the reptation regime when polymers become globally stiffer (Faller and Müller-Plathe, 2008). Thus our results suggest that chromatin persistence length globally increases on DSBs.

Global changes of chromatin mobility on DNA damage is an intriguing phenomenon, and over the last five yeasts, several views to explain it have been proposed in the literature. They can be grouped into two classes: 1) Global increase in chromatin motion is solely due to changes of external mechanical constrains that maintain chromatin and 2) global increase in chromatin motion is due to intrinsic chromatin modifications. To support the first view, several groups have studied the effect of centromere or telomere release on chromatin mobility. They found that centromere or telomere release alone gives a modest increase in mobility and are not sufficient to increase mobility of midarm chromosomes (Strecker *et al.*, 2016; Herbert *et al.*, 2017; Lawrimore *et al.*, 2017). However, Strecker *et al.* found that a combined disruption of telomeres and centromeres can reproduce chromatin mobility observed after a DSB (Strecker *et al.*, 2016); they identified the Mec1-dependent phosphorylation of Cep3, a kinetochore component, as an essential player in global increased chromatin mobility on DSBs. A different mechanism has been observed by Lawrimore *et al.*, who found that increased mobility of midarm chromosomes regions is microtubule dependent (Lawrimore *et al.*, 2017). In a sense, microtubules would be responsible for a global chromatin shake-up that would be essential for global increase mobility on DSBs (Lawrimore *et al.*, 2017).

The second view is that the intrinsic properties of chromatin are modified in response to DSBs, as proposed in the "altered chromatin model" (Miné-Hattab and Rothstein, 2013) and in Seeber *et al.* (2014). Chromatin state can be described by distinct parameters such as rigidity, compaction, and torsion. Changes in chromatin rigidity and compaction in response DNA damage have been recently discussed in the literature, however, with different conclusions. For example, a global chromatin decompaction/relaxation has been described in mammalian cells following DNA damage (Ziv *et al.*, 2006). More recently, the β-polymer model, as well as structured illumination microscopy imaging of a damaged locus, predicted chromatin expansion at the DSB in haploid yeast (Amitai *et al.*, 2017; Herbert *et al.*, 2017). Interestingly, 20–40% of the histones are degraded following DNA damage in haploid yeast: Such a loss of histones is proposed to globally increase chromatin decompaction and flexibility (Seeber *et al.*, 2014; Hauer *et al.*, 2017). However, this interpretation is still a matter of debate. Indeed, polymer models and STORM (stochastic optical reconstruction microscopy) imaging in haploid yeast has shown that global increased chromatin mobility on DNA damage is solely explained by an increase in chromatin rigidity without change in compaction (Herbert *et al.*, 2017). Phosphorylation of histone H2A, which can spread over 50 kb on both sides of a DSB (Lee *et al.*, 2014), contributes to the global increased mobility following DNA damage. Negative charges due to H2A phosphorylation might be the molecular basis of increased persistence length (Herbert *et al.*, 2017). As Herbert *et al.* used large levels of DSBs, it remains to be seen whether H2A phosphorylation in the presence of a single DSB would be enough to induce a global increase in persistence length and how it would be propagated to other chromosomes. All together, no consensus has yet been reached to explain the origin of global increased mobility after DNA damage. Our results support the model of a global increase in chromatin persistence length in reponse to DNA damage.

At the site of damage, we also observed crossing MSD curves and found that changes in mobility have a stronger effect compared with the rest of the genome (Figures 2 and 3 and Supplemental Figure S8). Unfortunately, we cannot easily interpret the MSD patterns observed close to the break in terms of persistence length using the Faller *et al.* study (Faller and Müller-Plathe, 2008) for several reasons. First, damaged DNA adopts different states from chromatin, ssDNA, repair proteins bound DNA, triple helix: These states have different physical properties (Fulconis *et al.*, 2006; Miné *et al.*, 2007). Second, damaged ends are surrounding by many repair proteins forming the repair focus (Lisby *et al.*, 2004). This compartment is more than 50 times more concentrated in repair proteins compared with the diffusive distribution of Rad52 in undamaged cells (Lisby and Rothstein, 2015). Polymer models treat DNA as a homogeneous fiber and local changes in the physical properties of polymers, or local changes in their environment, have not been investigated theoretically. Nevertheless, in vitro measurements have already shown that the persistence length of the Rad51-ssDNA nucleo-filament itself is increased, even in the presence of ATP where filaments are made up of small patches (Miné *et al.*, 2007; Lee *et al.*, 2013). Although the in vivo structure of the Rad51 nucleo-filament remains to be elucidated, the presence of Rad51 on the broken ends likely rigidifies DNA at the break. Moreover, in the absence of the Rad51 protein, we observe no change in mobility at both short and long time scales and no crossing MSD curves between damaged and undamaged loci (Figure 2E). Taken together, these findings underscore the role of Rad51 in local changes in stiffness at the DSB.

The "needle in a ball of yarn" model

Using our observations, we formulate a model in which DSBs modify chromatin mobility both locally and globally, enhancing long-distance explorations and minimizing local resampling. We propose that chromatin undergoes a genomewide increase in persistence length in response to DSBs. Moreover, the damaged locus undergoes an additional effect due to the binding of repair proteins, making changes in mobility more pronounced at the broken locus. By

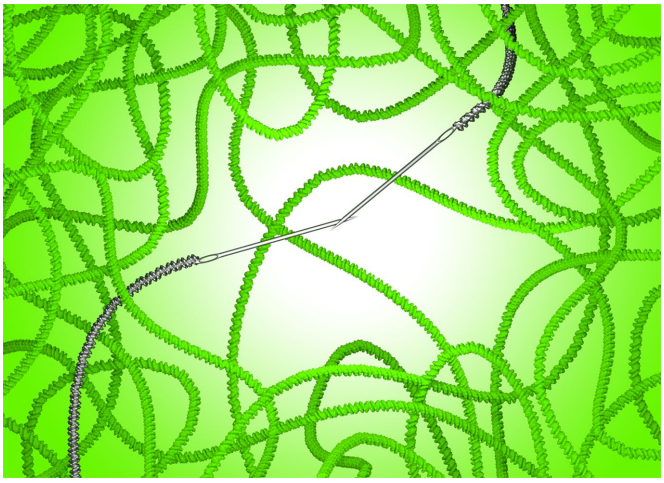

FIGURE 4: "Needle in a ball of yarn" model. To explain how chromatin exhibits decreased mobility at short time scales and simultaneously increased mobility at longer time scales after DNA damage, we propose the following model, which we call "needle in a ball of yarn." In response to double-strand breaks, chromatin undergoes a *genomewide increase in persistence length*. In addition, the damaged locus undergoes an additional effect due to the binding of repair proteins, making changes in mobility more pronounced at the broken locus. Following a DSB, the repair complex forms a nucleo-filament on the single-strand DNA tail, which stiffens the damaged end (here shown as a needle), thus decreasing its mobility locally. In a sense, DNA end acts like a "needle in a globally stiffer ball of yarn," enabling it to escape adjacent obstacles more efficiently, thus increasing mobility at longer time scales. Chromatin is depicted as a green helical fiber. The two ends are represented as searching together consistent with earlier observations (Lisby *et al.*, 2003; Kaye *et al.*, 2004; Lobachev *et al.*, 2004). The figure was realized by Myles Marshall.

stiffening the damaged DNA end, the repair machinery acts like a needle to help it search through the chromatin mesh, likened to a "ball of yarn" (Figure 4). At short time scales, the stiffening of the Rad51-bound DNA leads to a reduction of mobility. However, concomitantly, the Rad51-DNA nucleo-filament enhances its ability to pass through the chromatin meshwork and escape adjacent obstacles more efficiently as observed at larger scales. Overall global chromatin stiffening, combined with the "needle effect" at the DSB, facilitates the nuclear exploration of the damaged end throughout the genome, making it uniquely able to penetrate and explore the entangled chromatin network efficiently. Importantly, Rad51 is required for global changes in chromatin mobility/stiffness, indicating an essential role of the Rad51 proteins outside of the DSB in regulating global chromatin stiffening on DNA damage. Given the role of checkpoint proteins and chromatin remodelers in haploid cells (Dion *et al.*, 2012; Seeber *et al.*, 2013), it will be interesting to elucidate their contribution to regulate chromatin flexibility in diploid yeast.

More generally, our results illustrate that the different scales of chromatin organization translate into different scales in chromatin mobility that can be independently regulated. We propose that DNA diffusion is controlled by the local conformation of chromatin, that is, the level of entanglement as described in the "tube model" (De Gennes, 1982). Future studies with superresolution microscopy will allow the visualization of DNA organization at the nanoscale level in vivo to quantify how local and global DNA conformations are affected following damage (Recamier *et al.*, 2014; Ricci *et al.*, 2015). It will also be important to examine other biological processes at different time scales to see whether the multi-scale exploration of space that we observe here is a general property that allows a more efficient sampling of the environment.

MATERIALS AND METHODS

Strains

All strains used in this work are isogenic to *RAD5+* W303 derivatives (Zhao *et al.*, 1998) (Supplemental Table S2).

Cell culture and DSB induction

Before microscopy, cells were grown to early log phase in 4-ml cultures of synthetic culture (SC) medium + 100 mg/l adenine + 2% raffinose at 23°C overnight. In the morning, 2% galactose was added to the culture for 90 min to induce a single DSB at the I-*Sce*I cut-site. Cells were then pelleted, washed in SC + 100 mg/l adenine medium + 2% glucose to stop DSB induction, and placed on a 1.4% agarose slab for microscopy (Miné-Hattab and Rothstein, 2012). During the DSB induction, the I-*Sce*I cutting starts to occur after 30 min of induction, but the first Rad52 foci colocalizing with the *tetO* array are visible by microscopy after 90 min of induction and can last more than 30 min (Miné-Hattab and Rothstein, 2012). Thus the time of DSB formation cannot be known precisely. To measure DNA mobility of the damaged locus, we select cells harboring a Rad52 focus after 90 min of induction. The DSB is not necessarily formed at the same time in all cells examined: however, since we measure time-ensemble averaged MSDs on several cells, the presence of distinct anomalous regimes does not reflect different mobilities dependent on time after DSB induction but is solely due to the different time scales used to observe the locus.

Irradiation

Cells analyzed by microscopy were pregrown in SC + 100 mg/l of adenine + 2% glucose at 23°C overnight. Cells were then washed in the same media and exposed to 40 Gy of irradiation (x-rays, Yxlon International, Philipps). Irradiated cells were then immediately processed for imaging.

Microscopy

Imaging of single DNA loci was performed on an inverted microscope Nikon Ti Eclipse (Nikon Instruments, Tokyo, Japan), with a high numerical aperture objective (1.49 NA) and 100× magnification. We used a perfect focus system (Nikon) designed to avoid drift on the z-axis of the optical system and keep the cells in focus. The excitation laser beams (514 and 561 nm) were coupled to an optical fiber and focused in the back focal plane of the objective using an appropriate dual band dichroic (Semrock Di01-R488/561-25 × 36). Experiments were acquired with alternating pulsed excitation for the 514-nm laser and the 561-nm laser, respectively. Fluorescence emission from either YFP or RFP fluorescent proteins was filtered with a dual band emission filter with windows centered at 523 nm (45-nm bandpass) and 610 nm (45-nm bandpass) (Semrock FF01-523/610-25). The pixel size of the EMCCD (electron multiplying charge-coupled device) is 16 µm (iXon 897; Andor Technology, Belfast, Ireland), producing a pixel size of 160 nm after magnification. For the experiments at 5-ms acquisition time, we imaged a small region of interest containing the cell of interest, which allowed us to obtain acquisition rates as fast as 200 Hz (5 ms per frame).

All the experiments have been acquired with doses of light inferior to 0.2 J/cm^2 to protect cells from possible phototoxic effects (Logg *et al.*, 2009). All the experiments have been performed in the

same illumination conditions (see *Results* and Supplemental Figure S2).

Image analysis

We detected and tracked the *x* and *y* positions of the DNA loci using a homemade program inspired by the MTT tracking software (Serge *et al.*, 2008). From the *x* and *y* positions of the DNA locus over time, we computed the time-ensemble averaged MSD using the following formula: $MSD(\tau) = \langle \Delta \mathbf{r}(\tau)^2 \rangle = \langle [\mathbf{r}(t+\tau) - \mathbf{r}(t)]^2 \rangle$, where $\mathbf{r}(t)$ is the two-dimensional position of the particle at time t and τ is the lag time between two positions of the particle used to calculate the displacement $\Delta \mathbf{r}(\tau) = \mathbf{r}(t+\tau) - \mathbf{r}(t)$. The brackets, < >, are a time average over t and over locus trajectories acquired from different cells. The error bar is the 95% confidence interval.

We confirmed the anomalous nature of the motion using several methods (Supplemental Figure S3). The theoretical MSD of sub diffusive motion is a power law, $MSD(t) = At^{\alpha}$. However, experimental MSDs are altered from their theoretical shape due to various experimental limitations such as limited position accuracy or locus mobility during each image acquisition (Kepten *et al.*, 2013; Backlund *et al.*, 2015). Those limitations add an offset term, *b*, to the experimental asymptotic MSD, compared with the theoretical one: $MSD_{experimental}(t) = At^{\alpha} + b$ (Hughes, 1995) (see Supplemental Text 1). Here we derived a versatile formula of the MSD to compute this offset *b*, allowing us to accurately fit our experimental MSD derived from different acquisition schemes (see equation 1 from Supplemental Text 1 and Supplemental Figures S4 and S3). Our approach is more general than the one described in Kepten *et al.* (2013) since it also includes the exposure time as an additional parameter.

ACKNOWLEDGMENTS

We thank Leonid Mirny, Angela Taddei, Maxime Dahan, and Yaron Shav-Tal for fruitful discussions about this work. We also thank Eldad Kepten, Peter Thorpe, and Chloé Guedj for fruitful comments on the manuscript. This work was funded by a Marie Curie International Outgoing Fellowship (J.M.-H.), Agence Nationale de la Recherche (ANR)-12-PDOC-0035-01 (J.M.-H.), the Fondation pour la Recherche Médicale (Foundation for Medical Research in France) (V.R.), and the National Institutes of Health (GM50237, GM67055, and GM118180 to R.R.).

REFERENCES

Amitai A, Seeber A, Gasser SM, Holcman D (2017). Visualization of chromatin decompaction and break site extrusion as predicted by statistical polymer modeling of single-locus trajectories. Cell Rep 18, 1200–1214.

Andrews SS (2014). Methods for modeling cytoskeletal and DNA filaments. Phys Biol 11, 011001.

Backlund MP, Joyner R, Moerner WE (2015). Chromosomal locus tracking with proper accounting of static and dynamic errors. Phys Rev E Stat Nonlin Soft Matter Phys 91, 062716.

Backlund MP, Joyner R, Weis K, Moerner WE (2014). Correlations of three-dimensional motion of chromosomal loci in yeast revealed by the double-helix point spread function microscope. Mol Biol Cell 25, 3619–3629.

Barkai E, Garini Y, Metzler R (2012). Strange kinetics of single molecules in living cells. Phys Today 65, 29–35.

Ben-Avraham DHS (2000). Diffusion and Reactions in Fractals and Disordered Systems, Cambridge, UK: Cambridge University Press.

Bronshtein Berger I, Kepten E, Garini Y (2013). Single-particle tracking for studying the dynamic properties of genomic regions in live cells. Methods Mol Biol 1042, 139–151.

Bronstein I, Israel Y, Kepten E, Mai S, Shav-Tal Y, Barkai E, Garini Y (2009). Transient anomalous diffusion of telomeres in the nucleus of mammalian cells. Phys Rev Lett 103, 018102.

Burnecki K, Kepten E, Janczura J, Bronshtein I, Garini Y, Weron A (2012). Universal algorithm for identification of fractional Brownian motion. A case of telomere subdiffusion. Biophys J 103, 1839–1847.

Chiolo I, Minoda A, Colmenares SU, Polyzos A, Costes SV, Karpen GH (2011). Double-strand breaks in heterochromatin move outside of a dynamic HP1a domain to complete recombinational repair. Cell 144, 732–744.

Condamin S, Benichou O, Klafter J (2007). First-passage time distributions for subdiffusion in confined geometry. Phys Rev Lett 98, 250602.

De Gennes PG (1982). Kinetics of diffusioncontrolled processes in dense polymer systems. II. Effects of entanglements. J Chem Phys 76, 3322–3326.

Dimitrova N, Chen YC, Spector DL, de Lange T (2008). 53BP1 promotes non-homologous end joining of telomeres by increasing chromatin mobility. Nature 456, 524–528.

Dion V, Kalck V, Horigome C, Towbin BD, Gasser SM (2012). Increased mobility of double-strand breaks requires Mec1, Rad9 and the homologous recombination machinery. Nat Cell Biol 14, 502–509.

Faller R, Müller-Plathe F (2008). Chain stiffness intensifies the reptation characteristics of polymer dynamics in the melt. ChemPhysChem 2, 180–184.

Fulconis R, Mine J, Bancaud A, Dutreix M, Viovy JL (2006). Mechanism of RecA-mediated homologous recombination revisited by single molecule nanomanipulation. EMBO J 25, 4293–4304.

Guerin T, Benichou O, Voituriez R (2012). Non-Markovian polymer reaction kinetics. Nat Chem 4, 568–573.

Guerin T, Levernier N, Benichou O, Voituriez R (2016). Mean first-passage times of non-Markovian random walkers in confinement. Nature 534, 356–359.

Hajjoul H, Mathon J, Ranchon H, Goiffon I, Mozziconacci J, Albert B, Carrivain P, Victor JM, Gadal O, Bystricky K, *et al.* (2013). High-throughput chromatin motion tracking in living yeast reveals the flexibility of the fiber throughout the genome. Genome Res 23, 1829–1838.

Hauer MH, Seeber A, Singh V, Thierry R, Sack R, Amitai A, Kryzhanovska M, Eglinger J, Holcman D, Owen-Hughes T, *et al.* (2017). Histone degradation in response to DNA damage enhances chromatin dynamics and recombination rates. Nat Struct Mol Biol 24, 99–107.

Herbert S, Brion A, Arbona J-M, Lelek M, Veillet A, Lelandais B, Parmar J, Garcia Fernandez F, Almayrac E, Khalil Y, *et al.* (2017). Chromatin stiffening underlies enhanced locus mobility after DNA damage in budding yeast. EMBO J 36, 2595–2608.

Heun P, Laroche T, Shimada K, Furrer P, Gasser SM (2001). Chromosome dynamics in the yeast interphase nucleus. Science 294, 2181–2186.

Hughes BD (1995). Random Walks and Random Environments: Volume 1: Random Walks, Oxford, UK: Oxford Science Publications.

Jakob B, Splinter J, Conrad S, Voss KO, Zink D, Durante M, Lobrich M, Taucher-Scholz G (2011). DNA double-strand breaks in heterochromatin elicit fast repair protein recruitment, histone H2AX phosphorylation and relocation to euchromatin. Nucleic Acids Res 39, 6489–6499.

Kaye JA, Melo JA, Cheung SK, Vaze MB, Haber JE, Toczyski DP (2004). DNA breaks promote genomic instability by impeding proper chromosome segregation. Curr Biol 14, 2096–2106.

Kepten E, Bronshtein I, Garini Y (2013). Improved estimation of anomalous diffusion exponents in single-particle tracking experiments. Phys Rev E Stat Nonlin Soft Matter Phys 87, 052713.

Lawrimore J, Barry TM, Barry RM, York AC, Friedman B, Cook DM, Akialis K, Tyler J, Vasquez P, Yeh E, *et al.* (2017). Microtubule dynamics drive enhanced chromatin motion and mobilize telomeres in response to DNA damage. Mol Biol Cell 28, 1701–1711.

Lee CS, Lee K, Legube G, Haber JE (2014). Dynamics of yeast histone H2A and H2B phosphorylation in response to a double-strand break. Nat Struct Mol Biol 21, 103–109.

Lee M, Lipfert J, Sanchez H, Wyman C, Dekker NH (2013). Structural and torsional properties of the RAD51-dsDNA nucleoprotein filament. Nucleic Acids Res 41, 7023–7030.

Lisby M, Antunez de Mayolo A, Mortensen UH, Rothstein R (2003). Cell cycle-regulated centers of DNA double-strand break repair. Cell Cycle 2, 479–483.

Lisby M, Barlow JH, Burgess RC, Rothstein R (2004). Choreography of the DNA damage response: spatiotemporal relationships among checkpoint and repair proteins. Cell 118, 699–713.

Lisby M, Rothstein R (2015). Cell biology of mitotic recombination. Cold Spring Harb Perspect Biol 7, a016535.

Lobachev K, Vitriol E, Stemple J, Resnick MA, Bloom K (2004). Chromosome fragmentation after induction of a double-strand break is an active process prevented by the RMX repair complex. Curr Biol 14, 2107–2112.

Logg K, Bodvard K, Blomberg A, Kall M (2009). Investigations on light-induced stress in fluorescence microscopy using nuclear localization of the transcription factor Msn2p as a reporter. FEMS Yeast Res 9, 875–884.
Lucas JS, Zhang Y, Dudko OK, Murre C (2014). 3D trajectories adopted by coding and regulatory DNA elements: first-passage times for genomic interactions. Cell 158, 339–352.
Ma W, Resnick MA, Gordenin DA (2008). Apn1 and Apn2 endonucleases prevent accumulation of repair-associated DNA breaks in budding yeast as revealed by direct chromosomal analysis. Nucleic Acids Res 36, 1836–1846.
Maeshima K, Hihara S, Eltsov M (2010). Chromatin structure: does the 30-nm fibre exist in vivo? Curr Opin Cell Biol 22, 291–297.
Marshall WF, Straight A, Marko JF, Swedlow J, Dernburg A, Belmont A, Murray AW, Agard DA, Sedat JW (1997). Interphase chromosomes undergo constrained diffusional motion in living cells. Curr Biol 7, 930–939.
Masui O, Bonnet I, Le Baccon P, Brito I, Pollex T, Murphy N, Hupe P, Barillot E, Belmont AS, Heard E (2011). Live-cell chromosome dynamics and outcome of X chromosome pairing events during ES cell differentiation. Cell 145, 447–458.
Meister P, Gehlen LR, Varela E, Kalck V, Gasser SM (2010). Visualizing yeast chromosomes and nuclear architecture. Methods Enzymol 470, 535–567.
Metzler R, Jeon JH, Cherstvy AG, Barkai E (2014). Anomalous diffusion models and their properties: non-stationarity, non-ergodicity, and ageing at the centenary of single particle tracking. Phys Chem Chem Phys 16, 24128–24164.
Metzler R, Klafter J (2000). The random walk's guide to anomalous diffusion: a fractional dynamics approach. Phys Rep 339, 1–77.
Miné J, Disseau L, Takahashi M, Cappello G, Dutreix M, Viovy JL (2007). Real-time measurements of the nucleation, growth and dissociation of single Rad51-DNA nucleoprotein filaments. Nucleic Acids Res 35, 7171–7187.
Miné-Hattab J, Rothstein R (2012). Increased chromosome mobility facilitates homology search during recombination. Nat Cell Biol 14, 510–517.
Miné-Hattab J, Rothstein R (2013). DNA in motion during double-strand break repair. Trends Cell Biol 23, 529–536.
Misteli T (2010). Higher-order genome organization in human disease. Cold Spring Harb Perspect Biol 2, a000794.
Neumann FR, Dion V, Gehlen LR, Tsai-Pflugfelder M, Schmid R, Taddei A, Gasser SM (2012). Targeted INO80 enhances subnuclear chromatin movement and ectopic homologous recombination. Genes Dev 26, 369–383.
Perkins TT, Smith DE, Chu S (1994). Direct observation of tube-like motion of a single polymer chain. Science 264, 819–822.
Recamier V, Izeddin I, Bosanac L, Dahan M, Proux F, Darzacq X (2014). Single cell correlation fractal dimension of chromatin: a framework to interpret 3D single molecule super-resolution. Nucleus 5, 75–84.
Ricci MA, Manzo C, Garcia-Parajo MF, Lakadamyali M, Cosma MP (2015). Chromatin fibers are formed by heterogeneous groups of nucleosomes in vivo. Cell 160, 1145–1158.
Roukos V, Voss TC, Schmidt CK, Lee S, Wangsa D, Misteli T (2013). Spatial dynamics of chromosome translocations in living cells. Science 341, 660–664.
Saad H, Gallardo F, Dalvai M, Tanguy-le-Gac N, Lane D, Bystricky K (2014). DNA dynamics during early double-strand break processing revealed by non-intrusive imaging of living cells. PLoS Genet 10, e1004187.
Seeber A, Dion V, Gasser SM (2013). Checkpoint kinases and the INO80 nucleosome remodeling complex enhance global chromatin mobility in response to DNA damage. Genes Dev 27, 1999–2008.
Seeber A, Dion V, Gasser SM (2014). Remodelers move chromatin in response to DNA damage. Cell Cycle 13, 877–878.
Serge A, Bertaux N, Rigneault H, Marguet D (2008). Dynamic multiple-target tracing to probe spatiotemporal cartography of cell membranes. Nat Methods 5, 687–694.
Strecker J, Gupta GD, Zhang W, Bashkurov M, Landry MC, Pelletier L, Durocher D (2016). DNA damage signalling targets the kinetochore to promote chromatin mobility. Nat Cell Biol 18, 281–290.
Taddei A, Van Houwe G, Hediger F, Kalck V, Cubizolles F, Schober H, Gasser SM (2006). Nuclear pore association confers optimal expression levels for an inducible yeast gene. Nature 441, 774–778.
Therizols P, Duong T, Dujon B, Zimmer C, Fabre E (2011). Chromosome arm length and nuclear constraints determine the dynamic relationship of yeast subtelomeres. Proc Natl Acad Sci USA 107, 2025–2030.
Vasquez PA, Bloom K (2014). Polymer models of interphase chromosomes. Nucleus 5, 376–390.
Weber SC, Spakowitz AJ, Theriot JA (2010). Bacterial chromosomal loci move subdiffusively through a viscoelastic cytoplasm. Phys Rev Lett 104, 238102.
Zhao X, Muller EG, Rothstein R (1998). A suppressor of two essential checkpoint genes identifies a novel protein that negatively affects dNTP pools. Mol Cell 2, 329–340.
Ziv Y, Bielopolski D, Galanty Y, Lukas C, Taya Y, Schultz DC, Lukas J, Bekker-Jensen S, Bartek J, Shiloh Y (2006). Chromatin relaxation in response to DNA double-strand breaks is modulated by a novel ATM- and KAP-1 dependent pathway. Nat Cell Biol 8, 870–876.